Journal of Physics Research and Education, Volume 3, March 2026

Characterization of Two Members of the *N*-(*p-n-alkoxy benzylidene*)-*p-n-alkyl anilines* (nO.m) Series Using Complementary Experimental Techniques

Prabir Sarkar and Malay Kumar Das*
Department of Physics, North Bengal University, Siliguri 734013, West Bengal, India

Akhileshwar Prasad
Department of Physics, Siliguri College, Siliguri- 734001, India

In this study, we present a detailed investigation of the phase behavior of two homologues, namely 5O.12 and 5O.14, belonging to the series *N*-(*p-n-alkoxy benzylidene*)-*p-n alkyl anilines* (nO.m). A combination of high-resolution experimental techniques, including optical transmission, static dielectric permittivity, and modulated differential scanning calorimetry (MDSC), was employed to probe the isotropic–nematic (I–N), nematic–smectic A (N–SmA), and smectic A–smectic B (SmA–SmB) phase transitions. Temperature-dependent birefringence measurements indicate a progressive enhancement of orientational and bond-orientational ordering upon cooling. Dielectric studies reveal negative dielectric anisotropy, attributed to the lateral dipole moment associated with the $-\mathrm{C(H)}=\mathrm{N}-$ linkage within the molecular core. Calorimetric investigations, including heat-capacity anomalies and latent-heat evaluation, confirm the first-order character of all observed transitions. Furthermore, critical analysis based on renormalization-group (RG) scaling expressions yields critical exponent values (α) characteristic of weakly first-order behavior. The results highlight the significant role of terminal alkyl chain length in modulating mesomorphic properties and provide deeper insight into the molecular ordering processes governing higher-order smectic phase transitions.

I. INTRODUCTION

Liquid crystalline phases are broadly classified according to molecular organization within layers and the nature of interlayer correlations. In layered liquid crystal systems, a wide range of mesophases arises from different types of in-plane two-dimensional (2D) ordering combined with positional layering. These layered structures, characterized by long-range orientational order and varying degrees of in-plane positional correlation, are collectively known as smectic phases [1–5]. Understanding the transition behaviour among different smectic phases remains an important and challenging problem in soft condensed matter physics.

The present work focuses on selecting appropriate liquid crystalline materials that exhibit multiple higher-order smectic phases, thereby enabling a systematic investigation of the associated phase transitions using high-resolution techniques such as MDSC, optical birefringence, and dielectric permittivity measurements. In addition to investigating critical phenomena in various

* mkdnbu@nbu.ac.in

smectic phase transitions, the structural characterization of higher-ordered smectic phases is also of significant importance. The smectic B (SmB) phase is a layered structure with a hexagonal in-plane molecular arrangement. Experimental studies have identified two fundamentally distinct forms of the SmB phase [6–14]. The first type, commonly referred to as crystal B (CrB), exhibits true crystalline character. X-ray diffraction studies [14] reveal long-range three-dimensional (3D) positional order, and mechanical measurements confirm its solid-like behavior, as it can sustain shear stresses both within and between the layers. In contrast, the second variant of the SmB phase lacks interlayer positional correlations. It possesses short-range in-plane positional order but retains long-range three-dimensional six-fold bond-orientational order [15]. Mechanical investigations show that this phase cannot withstand in-plane shear stresses [16]. Owing to its hexatic symmetry, this form is designated as hexatic B (HexB).

In addition to the extensively studied isotropic–nematic (I–N) and nematic–smectic A (N–SmA) transitions, the present study emphasizes higher-order smectic phase transitions, particularly the SmA–SmB transformation. Since systematic investigations of critical behavior in higher-order smectic transitions remain relatively limited, transitions such as SmA–SmB, SmC–SmI, SmC–SmF, and SmI–SmF continue to attract considerable interest from both experimental and theoretical perspectives.

II. MATERIALS

A systematic physical investigation has been performed on two members of the homologous series *N*-(*p-n-alkoxy benzylidene*)-*p-n-alkyl anilines* (nO.m), where n and m denote the number of carbon atoms in the alkoxy and alkyl terminal chains, respectively. Compounds in this series exhibit nematic (N), smectic A (SmA), and smectic B (SmB) phases over well-defined temperature intervals. The selection of these two homologues from the same series enables a comparative study of how variations in terminal alkoxy and alkyl chain lengths influence their physical properties and phase behavior. The general molecular structure is shown in Fig. 1. The phase sequences

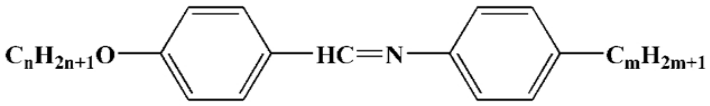

FIG. 1. The general molecular structure of the homologous series *N-(p-n-alkoxybenzylidene)-p-n-alkyl anilines (nO.m)*.

of the molecular structure are:
(i) **5O.12:** $n = 5, m = 12$
Phase sequence: Iso → 340.7 K → N → 338.6 K → SmA → 321.6 K → SmB

(ii) **5O.14:** $n = 5, m = 14$
Phase sequence: Iso → 344.5 K → N → 342.3 K → SmA → 324.7 K → SmB → 316 K → Cr

III. EXPERIMENTAL RESULTS

The experimental investigations on the two compounds were carried out using high-resolution techniques, namely Optical Transmission (OT), Static Dielectric Permittivity, and Modulated Differential Scanning Calorimetry (MDSC). These complementary measurements provide detailed insight into the optical characteristics of the mesophases as well as the thermodynamic nature and order of the associated phase transitions.

A. Birefringence measurements

The optical transmission method was employed to measure the optical birefringence (Δn) by analyzing the intensity of polarized light transmitted through a liquid crystal (LC) sample-filled cell coated with indium tin oxide (ITO) electrodes. The measurements were performed over a range of temperatures by recording the phase retardation ($\Delta\phi$) associated with the transmitted light intensity. Data acquisition was carried out at intervals of 3s, corresponding to a temperature resolution of approximately 0.025 K between successive points. Experimental details have been discussed elsewhere [17, 18]. The optical birefringence (Δn) was calculated using the relation

$$\Delta n = \frac{\lambda \Delta \phi}{2\pi d}, \tag{1}$$

where d is the LC cell thickness, $\Delta\phi$ is the phase retardation of the laser beam transmitted through the LC cell, and λ is the wavelength of the He–Ne laser beam. The sensitivity of the setup used for Δn measurements is estimated to be 5×10^{-5} for cells with a thickness of 5 μm. The temperature dependence of the optical birefringence (Δn) for the two mesogens 5O.12 and 5O.14 is shown in Fig. 2. All phase transitions present in these compounds are clearly visible, indicating the presence of a good monodomain sample throughout all mesophases during the measurement. After a discontinuity at the first-order transition from the isotropic phase, the birefringence increases rapidly with decreasing temperature due to the increase in the nematic order parameter. Upon further lowering the temperature, an enhancement in Δn occurs at the N–SmA phase transition. Such augmentation is attributed to the development of smectic-like short-range order within the nematic phase near the N–SmA transition, thereby further enhancing orientational order. Moreover, upon entering the low-temperature SmB phase, a further overall increase in Δn is observed. This increase is associated with the enhancement of bond-orientational order within the SmB phase near the SmA–SmB phase transition.

B. Static dielectric permittivity measurements

The temperature dependence of static permittivity ($\varepsilon_\perp$ and $\varepsilon_\parallel$), their average value (ε_{avg}), and dielectric anisotropy ($\Delta\varepsilon = \varepsilon_\parallel - \varepsilon_\perp$) for two compounds are measured using an Agilent LCR bridge [4294A] and shown in Fig. 3 [19]. The permittivity components ($\varepsilon_\perp$ and $\varepsilon_\parallel$) display different temperature-dependent behaviors. The $\varepsilon_\perp$ values initially increase as the temperature reduces from the isotropic phase and then decrease near the crystalline phase. In contrast with $\varepsilon_\perp$, the parallel component ($\varepsilon_\parallel$) shows the opposite trend. This results in a sign inversion of dielectric anisotropy ($\Delta\varepsilon$) close to the isotropic to nematic phase transition. Both compounds exhibit small

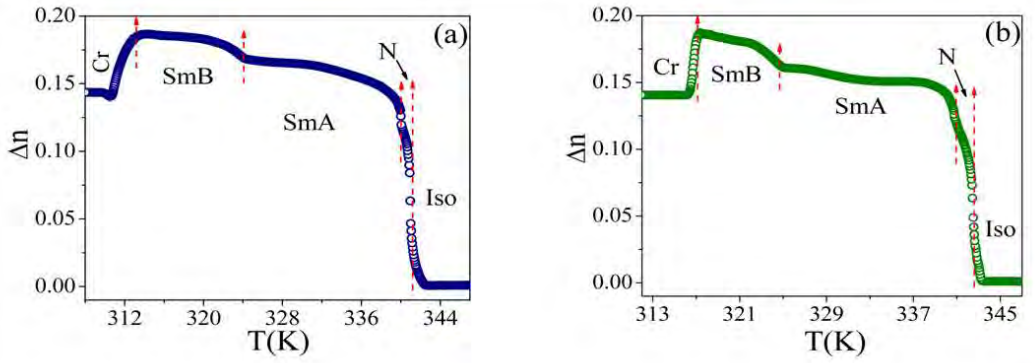

FIG. 2. Measured optical birefringence (Δn) vs temperature (T) of the compounds (a) 5O.12 (b) 5O.14; the dashed vertical arrow marks the different phase transition temperatures.

and negative values of dielectric anisotropy ($\Delta\varepsilon$). This negative dielectric anisotropy ($\Delta\varepsilon < 0$) is attributed to the development of a lateral dipole of the $-\mathrm{C(H)} = \mathrm{N}-$ central linkage group.

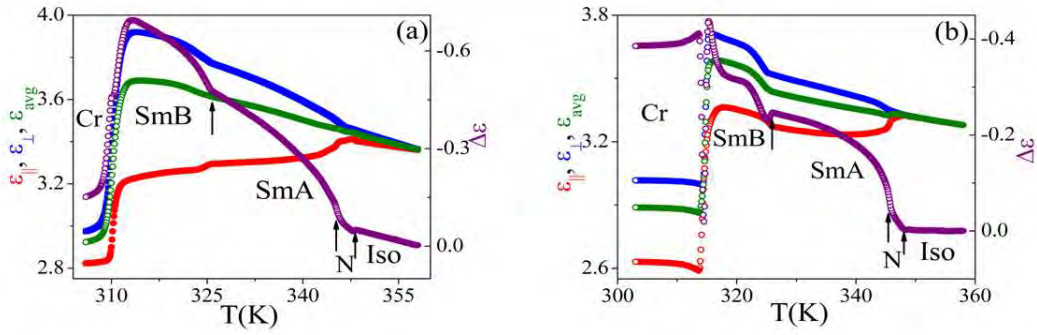

FIG. 3. Temperature variation of static dielectric permittivity components ($\varepsilon_{\parallel}, \varepsilon_{\perp}$), their average ($\varepsilon_{\mathrm{avg}}$) and the resulting dielectric anisotropy ($\Delta\varepsilon$) for: (a) 5O.12 and (b) 5O.14; solid arrows indicate the I-N phase transition; solid arrows indicate the higher-order smectic phase transition temperatures.

C. Calorimetric study

Thermal measurements were conducted using a commercial TA Instruments DSC-Q2000 system, equipped with a Refrigerated Cooling System (RCS), allowing temperature control in the range of 183 K to 823 K [17–19]. Fig. 4 shows the temperature-dependent specific heat capacity (ΔC_P), phase shift (δ) and imaginary part of heat capacity ($\Delta C_P''$) for studied compounds 5O.12 and 5O.14. It is evident that there is a significant change in the specific heat capacity and phase shift in the region of the I-N, N-SmA and SmA-SmB phase transitions, suggesting that all these transitions present in these compounds are first order. The imaginary parts of the heat capacity also justify the first-order nature of all the transitions. The latent heat (ΔH_L) can be directly determined from MDSC measurements performed in standard mode. Evaluation of the latent heat

associated with different phase transitions provides a preliminary indication of the thermodynamic nature of the transitions. Table I summarizes the calculated values of latent heat (ΔH_L) along with the corresponding total enthalpy change (ΔH_T) for the various phase transitions exhibited by the investigated compounds.

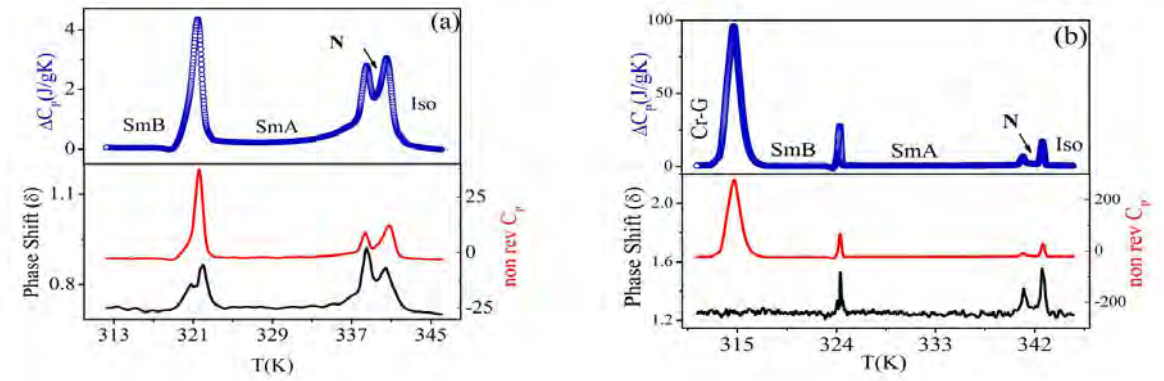

FIG. 4. Variation of heat capacity, phase shift, and imaginary part of heat capacity as a function of temperature for the compounds (a) 5O.12 and (b) 5O.14.

TABLE I. Calculated latent heat (ΔH_L) and total enthalpy (ΔH_T) for different phase transitions.

Compound	Phase Transition	Latent Heat (ΔH_L) (J/g)	Total Enthalpy (ΔH_T) (J/g)
5O.12	I-N	1.65	2.18
5O.12	N-SmA	0.98	1.15
5O.12	SmA-SmB	4.79	5.56
5O.14	I-N	3.91	5.90
5O.14	N-SmA	0.75	2.12
5O.14	SmA-SmB	6.71	8.96

IV. DISCUSSION

A. Critical behavior in the vicinity of different phase transitions

For a quantitative study of the critical behavior in the vicinity of different phase transitions, the temperature variation of excess heat capacity [$\Delta C_P = C_P - C_{P(\text{background})}$] data have been used [17–19]. Moreover, the temperature dependence of birefringence data has also been used to explore the critical behavior near these phase transitions. The birefringence data near the phase transitions for both the studied compounds show no visible discontinuity, and to find the exact transition temperature, the temperature derivative of Δn has been used. In order to examine better representation of the critical behavior near the phase transition, a new parameter having the

following form has been used [18, 19]:

$$Q(T) = -\frac{\Delta n(T) - \Delta n(T_C)}{T - T_C}, \tag{2}$$

where $\Delta n(T_C)$ is the birefringence at the transition temperature T_C. In an attempt to determine the critical exponent values and to study the critical behavior of the parameters $Q(T)$ and $\Delta C_P(T)$ data for different phase transitions, the following renormalization group expression, including the first-order corrections to scaling term has been used to fit the experimental data [20–22]:

$$Q(T) = \frac{A^{\pm}}{\alpha} |\tau|^{-\alpha} \left(1 + D^{\pm}|\tau|^{\Delta}\right) + F|\tau| + B^{\pm} \tag{2}$$

$$\Delta C_P(T) = \frac{A^{\pm}}{\alpha} |\tau|^{-\alpha} \left(1 + D^{\pm}|\tau|^{\Delta}\right) + B^{\pm}. \tag{3}$$

Here τ represent reduced temperature $\left(\frac{T-T_C}{T_C}\right)$, T_C represents phase transition temperature, $\pm$ denote above and below T_C, $A^{\pm}$ indicate the critical amplitudes and $D^{\pm}$ are the constants representing the first correction to scaling terms while Δ is the first correction to scaling exponent, $B^{\pm}$ represent the combined critical and regular background constants, and F presents the temperature-dependent contribution of the regular background.

B. Isotropic-Nematic phase transition

The study of pre-transitional behavior at the I-N transition has attracted interest, and various techniques have been employed for this purpose. In the isotropic phase, far away from the I-N transition temperature, the variation of the transmitted intensity is linear. However, near the transition, a nonlinear behavior in the temperature dependence of the transmitted intensity is observed. The results of specific heat capacity and birefringence (listed in Table II) across the I-N transition in compounds 5O.12 and 5O.14 indicate the first-order nature of this transition. The anomalous behavior in these parameters at the I-N transition Fig. 5 arises from the transition of a disordered molecular arrangement in the isotropic phase to an ordered molecular arrangement in the nematic phase. At the I-N transition temperature corresponding to the sharp change of birefringence (Δn), this change is consistent with the values obtained by other experimental techniques, such as the MDSC measurement.

TABLE II. Results of the excess specific heat capacity data (ΔC_P) and $Q(T)$, near the Iso-N phase transitions

Compound	A^-/A^+	D^-/D^+	α
5O.12	1.542±0.029	1.072±0.926	0.517±0.0342
5O.14	1.538±0.801	1.113±0.696	0.515±0.0391
Compound	A^-/A^+	D^-/D^+	α'
5O.12	1.525±0.0596	1.028±0.900	0.518±0.0598
5O.14	1.506±0.001	1.158±0.695	0.507±0.0214

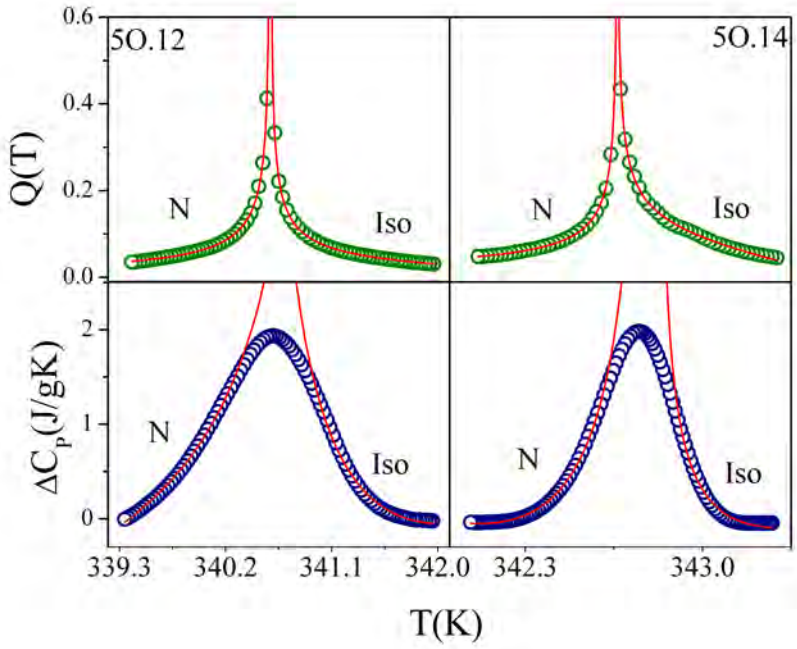

FIG. 5. Plot of $Q(T)$ and $\Delta C_P(T)$ as a function of temperature (T) for compounds 5O.12 and 5O.14 near the I-N phase transitions. The red solid lines indicate a fit to Eq. (3).

C. Nematic-Smectic A phase transition

The present work aims to elucidate the nature of the N–SmA phase transition in the investigated compounds. For compounds 5O.12 and 5O.14, the McMillan ratios (T_{NA}/T_{IN}) are found to be approximately 0.993 and 0.994, respectively. The very narrow nematic temperature range ($\sim$2 K) suggests a predominantly first-order character for the N–SmA transition. Furthermore, the transition is accompanied by a finite latent heat, pronounced anomalies in the heat capacity (ΔC_P), a distinct phase-shift peak (δ), and marked increases in birefringence (Δn) and dielectric anisotropy ($\Delta\varepsilon$). These experimental signatures collectively indicate that the N-SmA transition in both compounds exhibits first-order behavior. The temperature dependence of ΔC_P and $Q(T)$ in the immediate vicinity of the N-SmA phase transition is illustrated in Fig. 6. The average critical exponents obtained for the two compounds are approximately 0.511 and 0.512 (Table III), further corroborating the weakly first-order nature of the transition.

D. Smectic A-Smectic B phase transition

The nature of the SmA–SmB phase transition is not yet conclusively established and is characterized by unusual values of the associated critical parameters. In particular, the reported values of the specific heat critical exponent (α) vary widely, ranging from 0.48 to 0.68, while the experimentally determined order parameter exponent (β) lies between 0.15 and 0.25 [23–26]. Initially, the relatively large α values, close to 0.5, were interpreted as indicative of tricritical behavior. However, no clear evidence of a continuous crossover from 3D XY to tricritical behavior has been

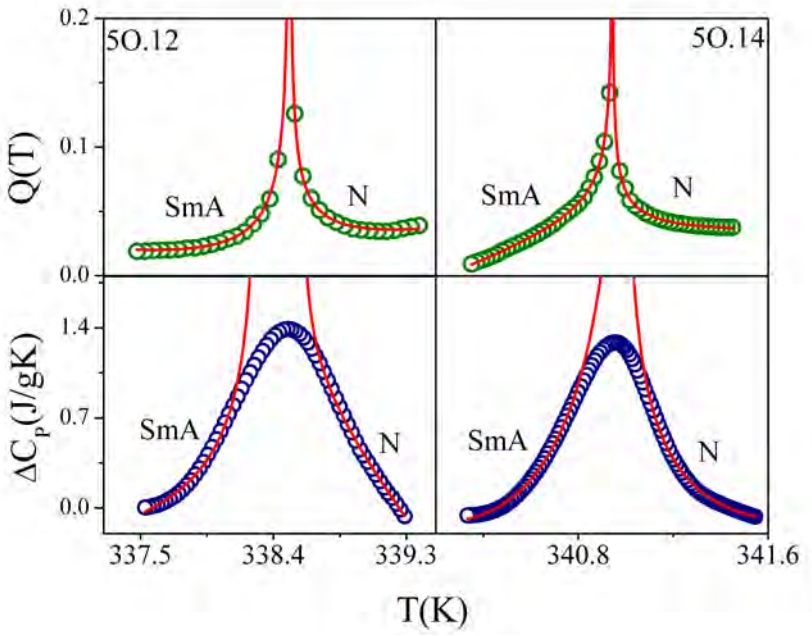

FIG. 6. Plot of $Q(T)$ and $\Delta C_P(T)$ as a function of temperature (T) for compounds 5O.12 and 5O.14 near the N-SmA phase transitions. The red solid lines indicate a fit to Eq. (3).

TABLE III. Results of the excess specific heat capacity data (ΔC_P) and $Q(T)$, near the N-SmA phase transitions

Compound	A^-/A^+	D^-/D^+	α
5O.12	1.581±0.029	1.12±0.926	0.511±0.0342
5O.14	1.588±0.801	1.03±0.696	0.505±0.0391
Compound	A^-/A^+	D^-/D^+	α'
5O.12	1.575±0.059	1.02±0.900	0.511±0.0598
5O.14	1.560±0.001	1.08±0.695	0.512±0.0214

observed, nor has any systematic correlation been established between the α values and the temperature width of the less ordered phase. At the same time, it has been definitively demonstrated that the SmA-SmB transition can exhibit first-order character.

Compounds 5O.12 and 5O.14 offer an opportunity to examine the critical behavior in the immediate vicinity of the SmA-SmB transition (Fig. 7). The critical exponents obtained from two independent experimental techniques, analyzed using renormalization group expressions, yield an α value of approximately 0.55 (Table IV). This value clearly supports the first-order nature of the transition. Upon cooling from the SmA to the SmB phase, a three-dimensional positional order develops in addition to the existing short-range translational order. The coupling between these two types of ordering is likely responsible for driving the SmA-SmB transition toward a first-order character.

The present study further evaluates the order parameter critical exponent (β) from the enhancement of birefringence (Δn) across the SmA-SmB transition in the 5O.12 and 5O.14 mesogens.

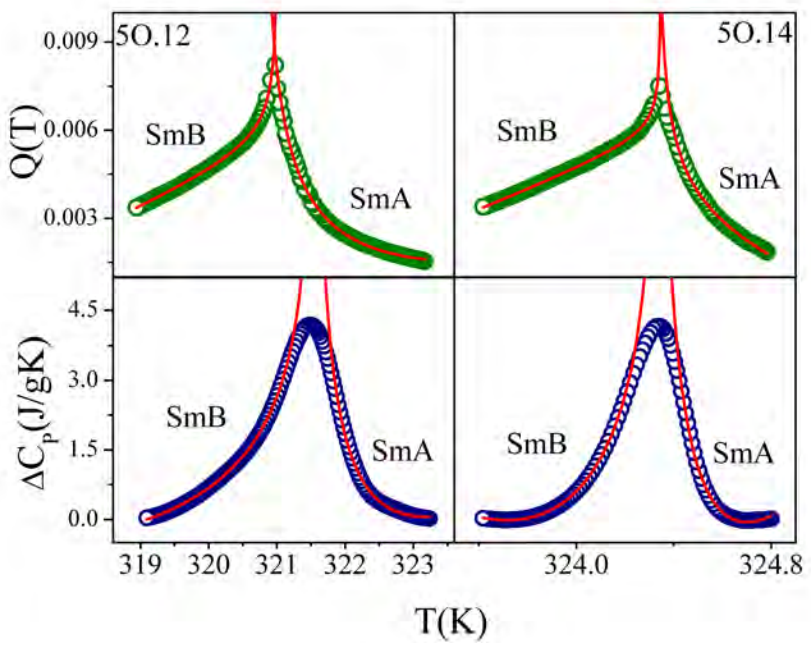

FIG. 7. Plot of $Q(T)$ and $\Delta C_P(T)$ as a function of temperature (T) for compounds 5O.12 and 5O.14 near the SmA-SmB phase transitions. The red solid lines indicate a fit to Eq. (3).

TABLE IV. Results of the excess specific heat capacity data (ΔC_P) and $Q(T)$, near the SmA-SmB phase transitions

Compound	A^-/A^+	D^-/D^+	α
5O.12	1.574±0.029	1.172±0.926	0.553±0.0342
5O.14	1.518±0.801	1.113±0.696	0.562±0.0391
Compound	A^-/A^+	D^-/D^+	α'
5O.12	1.585±0.0596	1.028±0.900	0.558±0.0598
5O.14	1.536±0.001	1.058±0.695	0.556±0.0214

For convenience, the value of Δn is set to zero, 2.5 degrees above the SmA-SmB transition temperature (T_C). For $T > T_C$, the variation of $|\delta(\Delta n)| = |\Delta n - \Delta n_0|$ is fitted to the form $C|\tau|^{(1-\alpha_1)}$ near the SmA-SmB phase transition. However, for $T < T_C$, both fluctuations and long-range order contribute to $\delta(\Delta n)$. The exponent β is extracted using $|\delta(\Delta n)| = D|\tau|^{2\beta} - C_1|\tau|^{(1-\alpha_1)}$, where D is a constant [26]. The first term is the long-range order contribution, and the second term is the fluctuation contribution to $\delta(\Delta n)$. The log-log plots of $\delta(\Delta n)$ above and below T_C for compounds 5O.12 and 5O.14 are shown in Figs. 8(a)–(b). The corresponding fitted parameters obtained from the analysis are summarized in Table V.

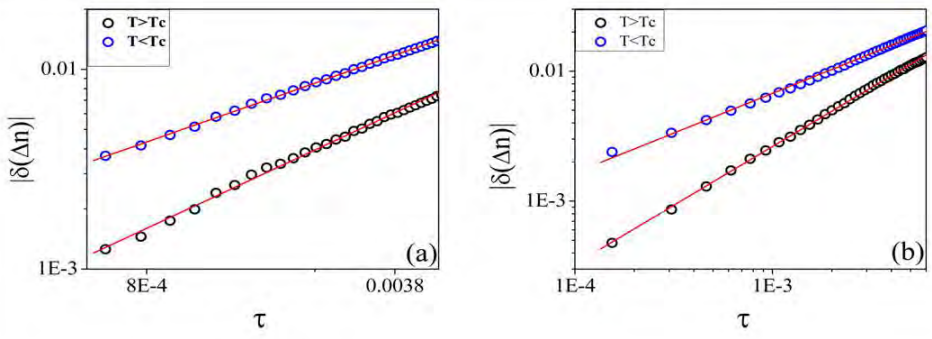

FIG. 8. Log-log plot of $|\delta(\Delta n)|$ vs reduced temperature (τ) for $T > T_C$ and $T < T_C$ (a) for compound 5O.12 and (b) for compound 5O.14. Solid lines indicate the linear fit to the data points.

TABLE V. The best-fitted parameter values were obtained in the presence of fluctuations and long-range order contribution near the SmA–SmB phase transition from optical birefringence measurements.

Compound	$(1-\alpha)$	β	A^-/A^+
5O.12	0.347 ± 0.008	0.271 ± 0.002	1.542 ± 0.029
5O.14	0.345 ± 0.005	0.290 ± 0.003	1.536 ± 0.017

V. CONCLUSION

A detailed experimental investigation of the liquid crystalline compounds 5O.12 and 5O.14 has been performed using optical birefringence, dielectric permittivity, and calorimetric measurements. The I–N, N–SmA, and SmA–SmB transitions all exhibit clear first-order characteristics, as evidenced by finite latent heat, birefringence discontinuities, and pronounced dielectric anomalies. Critical exponent analysis of excess heat capacity and birefringence data indicates that these transitions are weakly first-order. Both compounds exhibit negative dielectric anisotropy, arising from the lateral dipole moment associated with the Schiff-base linkage. A comparative assessment of the two homologues reveals that variation in terminal chain length subtly modifies transition temperatures and the degree of molecular ordering. Overall, these results provide deeper insight into the formation of higher-order smectic phases and establish reliable experimental benchmarks for theoretical descriptions of phase behavior in liquid crystalline materials.

Acknowledgement : PS gratefully acknowledges the Council of Scientific and Industrial Research, New Delhi [09/285(0098)/2020-EMR-I] for financial support through a Senior Research Fellowship. MKD acknowledges funding from the Anusandhan National Research Foundation (ANRF), New Delhi, under Grant No. (ANRF/IRG/2024/000515/PS). The authors also sincerely thank Prof. Parameswara Rao Alapati for kindly providing the samples used in this study.

[1] O. D. Lavrentovich, Liq. Cryst. Today **4**, 7 (1994).
[2] G. W. Gray *et al.*, *Smectic Liquid Crystals: Textures and Structures* (Leonard Hill, 1984).

[3] I. Dierking, *Texture of Liquid Crystals* (Vasa, 2008).
[4] P. G. De Gennes, *The Physics of Liquid Crystals* (Clarendon Press, Oxford, 1974).
[5] P. G. De Gennes, Mol. Cryst. Liq. Cryst. **21**, 49 (1973).
[6] W. H. De Jeu *et al.*, Rev. Mod. Phys. **75**, 181 (2003).
[7] K. Vikram *et al.*, Spectrochim. Acta A **75**, 1480 (2010).
[8] J. W. Goodby and R. Pindak, Mol. Cryst. Liq. Cryst. **75**, 233 (1981).
[9] P. S. Pershan, Int. Tables Crystallogr. **B**, 460 (2006).
[10] P. D. Roy *et al.*, Mol. Cryst. Liq. Cryst. **457**, 43 (2006).
[11] A. Deptuch *et al.*, Liq. Cryst. **52**, 157 (2025).
[12] M. K. Usha and N. Bharathi, Int. J. Sci. Eng. Sci. **2**, 17 (2018).
[13] M. K. Usha *et al.*, Mol. Cryst. Liq. Cryst. **623**, 9 (2015).
[14] M. K. Das *et al.*, Mol. Cryst. Liq. Cryst. **457**, 55 (2006).
[15] R. P. Kurta *et al.*, Phys. Rev. Lett. **110**, 044501 (2013).
[16] R. Pindak *et al.*, Phys. Rev. Lett. **48**, 173 (1982).
[17] P. Sarkar *et al.*, Liq. Cryst. **52**, 1313 (2025).
[18] P. Sarkar *et al.*, Eur. Phys. J. E **47**, 44 (2024).
[19] P. Sarkar *et al.*, Phase Transitions **99**, 76 (2026).
[20] A. Chakraborty *et al.*, Phys. Rev. E **91** (2015).
[21] A. Chakraborty *et al.*, Phys. B **479**, 90 (2015).
[22] B. Barman *et al.*, Liq. Cryst. **51**, 1523 (2024).
[23] C. Rosenblatt and J. T. Ho, Phys. Rev. A **26**, 2294 (1982).
[24] G. Nounesis *et al.*, Phys. Rev. Lett. **56**, 1712 (1986).
[25] F. Mercuri *et al.*, Phys. Rev. E **68**, 051705 (2003).
[26] H. Haga and C. W. Garland, Phys. Rev. E **57**, 603 (1998).